

Cerebrospinal Fluid Shunts: Flow Measurements with MR Imaging¹

The authors describe a technique for determination of shunt patency by quantifying cerebrospinal fluid shunt flow rates with magnetic resonance (MR) imaging. This method uses a modified clinical sequence that is both sensitive to slow flow perpendicular to the imaging plane and capable of achieving oblique angles with a 4-cm field of view. Velocity-dependent phase images were used to quantify flow rates within the shunt. A preliminary study was performed in seven patients with hydrocephalus and cerebrospinal fluid shunts. Two patients were found to have zero flow in the shunt, while the remaining five had flow rates ranging from 4 to 19 mL/h. Results showed that the measurement of flow rates within the shunt lumen with MR imaging is clinically feasible.

Index terms: Brain, hydrocephalus, 10.82 • Cerebrospinal fluid, flow dynamics, 10.1214 • Cerebrospinal fluid, MR studies, 10.1214 • Magnetic resonance (MR), physics • Magnetic resonance (MR), technology • Shunts, ventricular, 10.451

Radiology 1989; 173:243-247

¹ From the Department of Medical Biophysics, Ontario Cancer Institute, University of Toronto, 500 Sherbourne St, Toronto, Ont, Canada, M4X 1K9 (A.J.M., R.M.H.); Department of Neurosurgery, Hospital for Sick Children, University of Toronto (J.M.D.); and MR Laboratory, Toronto Western Hospital (C.L.). Received February 2, 1989; revision requested March 29; revision received May 1; accepted May 30. Supported by the University Research Incentive Fund (Ontario), GE Medical Systems Canada, and the Appugliesi Fund. A.J.M. supported by a Natural Sciences and Engineering Research Council (Canada) studentship. Address reprint requests to A.J.M.

© RSNA, 1989

CEREBROSPINAL fluid (CSF) is produced predominantly by the choroid plexus at a rate of about 500 mL/d in adults (1). The CSF circulates through the ventricular system, usually in a pulsatile manner; exits from the outlet foramina of the fourth ventricle to enter the basal cisterns; and ultimately is absorbed by the arachnoid villi over the surface of the brain. Hydrocephalus, a state of excess accumulation of CSF, is caused by an obstruction to normal CSF flow patterns. This obstruction may occur in the ventricular system, in the subarachnoid pathways, or at the site of absorption into the venous system. The standard method of treating this condition is to implant a CSF shunt. A shunt is a thin cylindrical tube made of soft, silicone material and has a typical lumen diameter of 1.2 mm. The shunt frequently extends subcutaneously from the ventricles to a distal cavity, usually the peritoneum. Its purpose is to allow drainage of the excess CSF into a distal cavity where the fluid can be absorbed. The shunt has a valve to control flow and prevent contamination that could be caused by reflux. However, shunts frequently become occluded by debris and therefore stop functioning. Shunt malfunction can also be caused by improper placement, disconnection, breakage, migration, infection, and component malfunction (2). In a recent study, it was shown that shunt procedures were performed at a rate of 125/10⁶ people per year. Of these procedures, 38% were revisions of previously implanted shunts (3).

Patients with a malfunctioning shunt suffer symptoms such as lethargy, nausea and vomiting, headaches, and impaired cognitive and motor development as a result of the increase in intracranial pressure. These symptoms, however, can lead to several possible diagnoses; thus, a method of determining shunt paten-

cy is needed. Current screening techniques to determine shunt patency include injection of a radioactive tracer (4,5) or contrast agent (6), ultrasonographic (US) measurement during shunt pumping (7), and cooling of the CSF externally and detection of flow with a thermistor (8). There has also been a study in which an electrolysis unit was implanted and the resulting bubbles were tracked with US (9). Of these techniques, radionuclide imaging has become the primary clinical modality of choice because it is accurate and available. However, this modality is associated with the risk of shunt infection and exposure to a radioisotope. Magnetic resonance (MR) imaging has the potential to be a diagnostically accurate, noninvasive technique for determining shunt patency. This investigation demonstrates a clinically viable method of directly assessing shunt performance with in vivo MR imaging.

MATERIALS AND METHODS

The application of MR imaging to this diagnostic problem has several distinct challenges that must be addressed. The first of these is to achieve a field of view (FOV) small enough to be sensitive to the region within the 1.2-mm inner diameter of the shunt. The capability of achieving oblique angles at this FOV is also necessary to obtain true axial images of the shunt. Furthermore, with CSF production rates of about 500 mL/d, average flow rates within the shunt can be expected to be approximately 5 mm/sec. A flow technique must therefore be developed that is sensitive to these flow rates under the constraints placed by a reduced FOV.

All experiments were performed on a 1.5-T Signa imaging system (GE Medical Systems, Milwaukee). To view the shunt with a reasonable amount of resolution, a 4-cm FOV with a 256 × 256 matrix was

Abbreviations: CSF = cerebrospinal fluid, FOV = field of view.

chosen. This ensures a minimum of 32 pixels within the shunt lumen, which is sufficient to easily differentiate it from the surrounding tissue and to assess its function. The minimum FOV available on the Signa unit is 8 cm, primarily because of the limit of 10 mT/m on peak gradient strength. A 4-cm FOV could therefore not be achieved by increasing the gradient strength. Rather, the gradient strengths corresponding to an 8-cm FOV were employed, and the duration of the phase-encoding and readout gradients was doubled. A 4-cm FOV was thereby obtained by doubling the data acquisition time and reducing the bandwidth from ± 16 kHz to ± 8 kHz. This has an additional advantage over increased gradient strengths in that the noise in the image is reduced due to the reduced bandwidth (10). Because longer echo times are required with this approach, an echo time of 80 msec and repetition time of 500 msec were used. The relaxation times of CSF ($T_1 \approx 4$ sec, $T_2 \approx 2$ sec, [11]) allow this echo time without substantial signal loss.

A 4-cm FOV leads to difficulties with low signal-to-noise ratio, aliasing of surrounding tissue, and patient motion. To alleviate the first two problems, a special surface-coil receiver was developed (Fig 1). This coil was designed to follow the curve of the neck and was long and narrow to fit the shunt geometry. When tested against a standard 3-inch Signa surface coil, the shunt coil was found to have a threefold improvement in signal-to-noise ratio at a depth of 1 cm. The high sensitivity of the shunt coil over a short range also substantially reduced the problem of aliasing. A section thickness of 10 mm was chosen to improve the signal-to-noise ratio in the images. This section thickness, however, gives voxel dimensions of $0.16 \times 0.16 \times 10.0$ mm. With such a high-aspect ratio and irregular shunt paths in vivo, oblique angle imaging is essential. To facilitate oblique angle imaging with-

out exceeding the gradient limitations, a pulse sequence was designed so that no two gradients were active concurrently (Fig 2). Long echo times are also required in designing a sequence such as this one.

Phase images have been shown to be a useful tool for detecting and quantifying flow in an MR image (12-14). Phase sensitivity to flowing spins can be enhanced or suppressed as a function of the gradient waveforms (15-17). Spins moving perpendicular to the imaging plane accumulate phase as (12,13)

$$\Phi = 360 \cdot \gamma \int G_z \cdot Z(t) dt, \quad (1)$$

where Φ = accumulated phase in degrees, $Z(t) = z + v_z \cdot t + a_z \cdot t^2/2! + \dots$, G_z = section-select gradient waveform, and γ = gyromagnetic ratio for protons (42.57 MHz T^{-1}).

If the net waveform area is assumed to be zero—which is to say the area under G_z prior to the 180° radio-frequency pulse is exactly matched by the area after the 180° pulse—and acceleration or any higher order terms of motion are neglected, a simplified version of Equation (1) can be produced:

$$\Phi = 360 \cdot \gamma \int G_z \cdot v_z t dt. \quad (2)$$

Equation (2) gives the rate of accumulation of phase experienced by spins moving perpendicular to the imaging plane with velocity v_z and through a magnetic field gradient G_z . The section-select gradient (G_z) was modified in our shunt sequence by the addition of two lobes of equal area (Fig 2). These lobes produce a significant phase advance for spin velocities of the order of 5 mm/sec without the induced phase exceeding 360° . In practical imaging, stationary tissue does not actually collect a zero net phase due to limitations in the applied magnetic fields. Instead, the stationary tissue tends to produce a reference phase shift against which moving spins must be compared to obtain their net accumulated phase.

Both magnitude and phase images were produced from the acquired raw data. The magnitude image was used to produce a

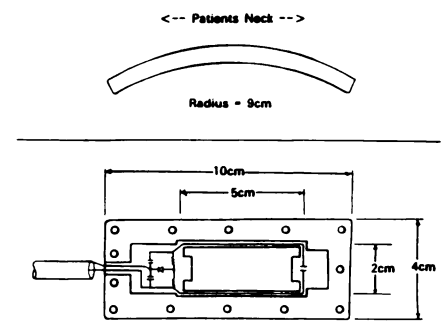


Figure 1. Schematic diagram of the shunt coil shows its geometry and the circuitry employed to match the coil to 50 Ω real at an operating frequency of 63.91 MHz.

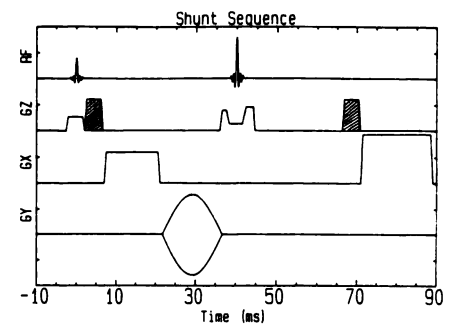


Figure 2. Modified clinical pulse sequence with extended phase encoding and readout gradient duration to allow a 4-cm FOV. The shaded lobes on the section-select gradient (G_z) produce a significant phase advance for velocities of the order of 5.0 mm/sec. The frequency-encoding (G_x) and phase-encoding (G_y) gradients have been extended to facilitate a 4-cm FOV. RF = radio-frequency pulses.

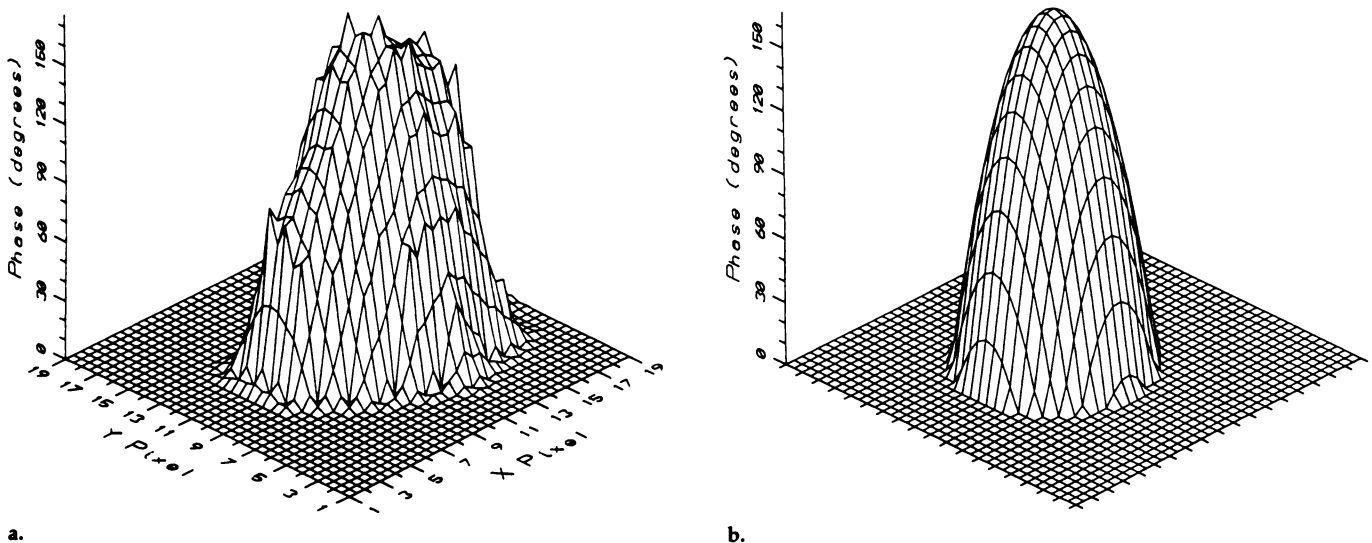


Figure 3. (a) Three-dimensional representation of the processed phase image of the shunt in patient 2, in which a flow rate of 19.0 mL/h was found. (b) Paraboloid structure seen in a is modeled to produce this surface from which the peak phase advance can be extracted.

template from which the integrity of the phase in each pixel was determined. Any pixel with low signal intensity on the magnitude image was flagged and disregarded in further processing. The remaining pixels on the phase image, minus the area within the shunt, were then mod-

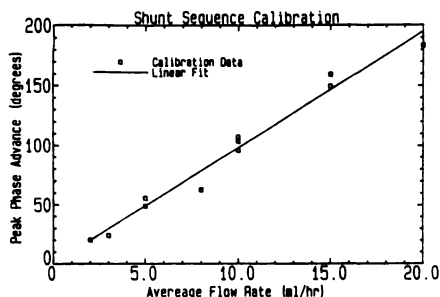
eled to a quadratic to determine the phase surface defined by stationary tissue. This surface was then subtracted from the phase data, which left nonzero phase only in regions of flow. The phase within the shunt was then modeled to a paraboloid to interpolate the peak phase ad-

vance (Fig 3).

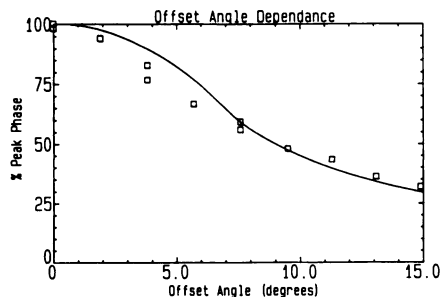
The technique was initially tested and calibrated on a phantom consisting of a shunt extending coaxially through a water-filled cylinder of 1.5-cm inner diameter. The water in the cylinder was stationary and acted as the background for the moving spins in the shunt. Water was infused into the shunt at a constant rate with a syringe infusion pump (Harvard Apparatus, South Natick, Mass). The shunt coil was placed on the outer cylinder, about 1.0 cm from the shunt. Imaging time was 8 minutes 32 seconds for four averages acquired to improve image quality. A calibration plot relating the average flow rate in the shunt to the interpolated peak phase advance was then produced (Fig 4). The effect of an incorrectly defined oblique imaging plane was also investigated with this phantom. A significant loss of phase advance was found when the imaging plane did not correspond to a true axial section of the shunt. This phenomenon is due to the skewed voxel dimensions employed with this technique. Voxels oriented at an angle relative to the velocity distribution within the shunt will contain a broader range of phase advances than correctly aligned voxels. Since the net phase of a voxel is a magnitude-weighted average of its constituent parts, an increase in this offset angle will produce an apparent reduction of the peak phase advance within the shunt (Fig 5). A secondary distortion of phase due to the development of flow in the frequency encoding direction may also affect the results (18). This strong dependence between peak phase shift and offset angle illustrates the necessity of a well-defined oblique plane when one is attempting to obtain accurate quantitative flow rates.

In the clinical environment, we found that a modified protocol was required. A general knowledge of the shunt location must initially be obtained by inspection. Placement of the shunt coil longitudinally along the shunt both provides a marker of its location and assures maximal signal from its interior. Initial axial images with a 24-cm FOV and subsequently an 8-cm FOV were required to locate the shunt path and thereby define an appropriate oblique plane. Shunts at very oblique angles can be hard to identify in these initial axial images due to blurring caused by finite section thicknesses and the small shunt diameter. To minimize this blurring, patients were set up so the shunt would extend in an approximately superior-inferior manner. The section thickness was also reduced to 5 mm in these localization images and an echo time of 20 msec was employed for improved image contrast. The flow-sensitive image with a 4-cm FOV was then obtained at an appropriate oblique plane.

A total of seven asymptomatic patients ranging in age from 15 to 40 years with shunts implanted to treat hydrocephalus were tested with the technique. Some attempt was made to determine whether these patients had functional shunts. Two

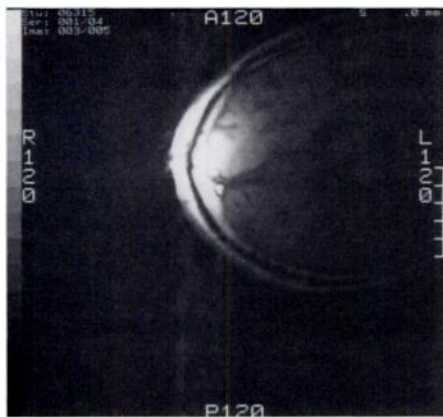


4.

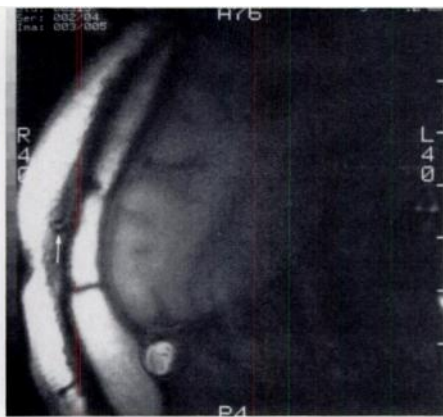


5.

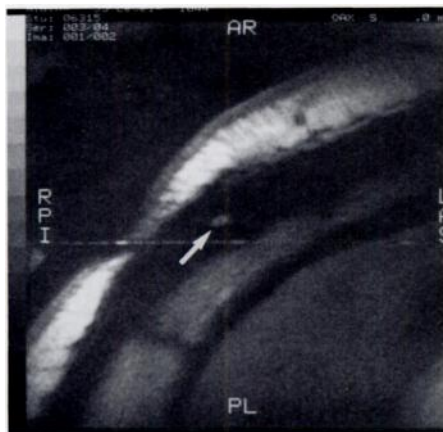
Figures 4, 5. (4) Calibration plot of the peak accumulated phase as interpolated from the phase image to the average flow rate infused into the shunt phantom. (5) Theoretical and experimental demonstration of the effects of a misaligned oblique plane on peak phase advance within a shunt. Solid line represents the predicted loss of phase due to the broadening of the phase values of spins within a voxel. Inflection in the curve is due to the eventual averaging of surrounding tissue, which has a net accumulated phase of zero. Boxes represent the peak phase advance as a function of offset angle as measured on the shunt phantom.



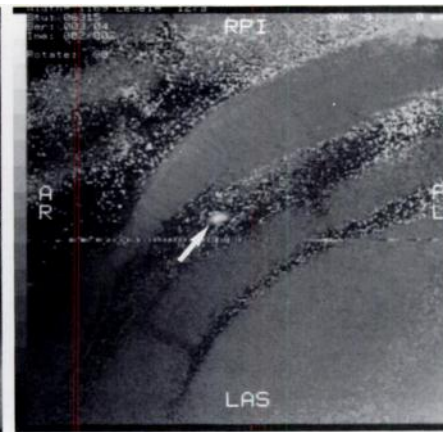
a.



b.



c.



d.

Figure 6. (a) Image of patient 2, obtained with a 24-cm FOV, was used to locate the shunt by means of the area of high signal intensity. (b) One of the 8-cm-FOV images used to locate the shunt and define the appropriate oblique plane. (Shunt location is indicated by arrow in b, c, and d.) (c) The 4-cm-FOV magnitude image used as a template for the corresponding phase image shown in d. (d) Phase image corresponding to c shows flow due to the increased phase values within the lumen of the shunt. A = anterior, I = inferior, L = left, R = right, S = superior.

patients had not undergone shunt revisions for 8 and 9 years each. Their hospital records also stated that the shunt appeared obstructed on the basis of manipulation of the shunt reservoir and surmising that these two patients had become shunt independent. The other five patients had undergone shunt revisions within the previous 2 years and were thought to be shunt dependent.

RESULTS

Figure 6 shows a complete study of one of the patients. Figure 6a is the initial image obtained to establish the general location of the shunt. It should be noted that the shunt is not visible in this 24-cm FOV and that the region of high signal intensity surrounding the shunt coil location is used as a marker. Figure 6b is one of the subsequent 8-cm-FOV images used to locate the shunt in several sections and thereby define an appropriate oblique plane. Figure 6c and 6d are the magnitude and phase images, respectively, obtained with the flow-sensitive sequence. Regions of low signal intensity on the magnitude image have a characteristic speckled pattern in the corresponding phase image due to a random accumulation of phase. The glowing dot corresponding to the location of the shunt on the phase image (Fig 6d) indicates the presence of flow and therefore patency of the shunt. Analysis of the phase in this image revealed a flow rate of 19.0 mL/h.

Flow within the shunt was measured in all seven of the patients tested. There was a wide variation in flow rates, with the extremes being 0 and 19.0 mL/h (Table 1). The magnitude of these values corresponds roughly to the flow rates that might be expected on the basis of the normal rate of CSF production. In a prior study, flow rates measured with an electrolysis unit ranged from 0.3 mL/h to 46.8 mL/h, which are also in qualitative agreement (9).

It should be noted that the flow within the shunt may be periodic, as is the case of CSF in the brain. In this case, the flow of CSF within the shunt would vary with the cardiac cycle. Respiratory oscillations, in addition to cardiac oscillations, may also govern shunt flow because the distal end of the shunt is located in the peritoneal cavity. The high resistance provided by the small radius of the shunt, however, should damp any rapid velocity fluctuations. A time-averaged flow rate of CSF will be achieved if sufficient sampling is performed to resolve all features of

the flow cycle (19). With an imaging time of over 8 minutes, (including four averages) and no attempt to gate the sequence, we are confident that the phase image produced represents an average of the flow rates within the shunt.

The two patients who were thought to have nonfunctioning shunts were found to have either no flow or a flow rate beneath the sensitivity of this technique (Fig 7). This is illustrated in Figure 7b, as the phase within the lumen of the shunt lies on the phase surface defined by the surrounding stationary tissue. The noise in the phase image makes flow rates of less than 2 mL/h difficult to detect accurately. Slower flow may be detected by increasing the amplitude of the additional lobes on the section-select gradient waveform; however, the maximum phase detectable without wraparound would also be reduced. A second image with increased flow sensitivity may prove worthwhile in cases in which flow cannot clearly be deciphered in the initial image.

DISCUSSION

A quantitative method of determining CSF flow within the lumen of a shunt has been described. The technique has been tested successfully with a phantom model, as well as in the clinical environment. Previously, Savader et al (20) published a report illustrating a flow-void effect in shunts with relatively high flow rates. The problem with a technique such as this is that it does not give quantitative flow information. Care also needs to be taken to ensure that the signal loss is due to a flow void and not to a susceptibility effect. The

use of phase images, however, allows quantitative flow analysis and improved sensitivity to slower flow rates. It would therefore appear that the phase-image approach is most appropriate in this case.

The measurement of flow within the lumen of a shunt may prove useful in assessing shunt patency. In cases in which a substantial flow rate is found, it would be safe to assume shunt patency. However, the meaning of a zero flow rate, as assessed with this technique, is still not clear. A zero flow reading could be explained by very slow flow of CSF, transient arrest of shunt flow, or a blockage in the shunt. Very slow flow could be detected by increasing the sensitivity of the technique, but periods of flow arrest longer than the imaging time could prove troublesome. Work therefore is currently being performed to determine the nature of flow in shunts with this technique.

The measurement of flow rates within the lumen of a shunt with MR imaging is a clinically feasible technique. Flow rates as low as 2 mL/h can be measured with the current technique, and lower flow rates could be detected with additional higher gradient images. Minimal ad-

Table 1
In Vivo Flow Rates in CSF Shunts

Patient No./Age (y)	Flow (mL/h)
1/30	4 ± 2
2/27	19 ± 2
3/10	10 ± 2
4/15	7 ± 2
5/40	5 ± 2
6/17	0 ± 2
7/17	0 ± 2

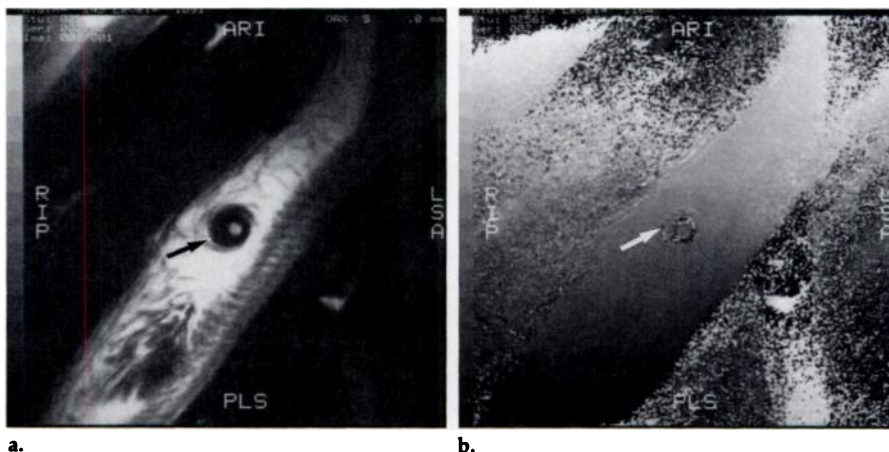


Figure 7. (a) The 4-cm-FOV magnitude image of the shunt and surrounding area (arrow) in patient 6. (b) Corresponding phase image shows no indication of flow within the shunt lumen (arrow).

aptation of clinical sequences and an appropriate surface coil are the only tools required to implement this technique. Total patient imaging times of less than 15 minutes and a patient throughput of two per hour are realistic goals. The success of the technique can be limited by patient motion and the difficulty of identifying shunts extending in highly oblique paths to the localization images. Similarly, the accuracy of flow rates depends on the correct determination of an appropriate oblique imaging plane. These limitations, however, can be minimized with appropriate setup in the clinical environment. ■

References

- Lorenzo AV, Page LK, Watters GV. Relationship between cerebrospinal fluid formation, absorption and pressure in human hydrocephalus. *Brain* 1970; 93:679-692.
- Walters BC, Hoffman HJ, Hendrick EB, Humphreys RB. Cerebrospinal fluid shunt infection. *J Neurosurg* 1984; 60:1014-1021.
- Hoffman HJ, Smith MSM. The use of shunting devices for cerebrospinal fluid in Canada. *Can J Neurol Sci* 1986; 13:81-87.
- Hayden PW, Rudd TG, Shurtleff DB. Combined pressure-radionuclide evaluation of suspected cerebrospinal fluid shunt malfunction: a seven-year clinical experience. *Pediatrics* 1980; 66:679-684.
- Howman-Giles R, McLaughlin A, Johnston I, Whittle I. A radionuclide method of evaluating shunt function and CSF circulation in hydrocephalus. *J Neurosurg* 1984; 61:604-605.
- Seppanen U, Serlo W, Saukkonen AL. Valvography in the assessment of hydrocephalus shunt function in children. *Neuroradiology* 1987; 29:53-57.
- Flitter MA, Buchheit WA, Murtagh F, Lappayowker MS. Ultrasound determination of cerebrospinal fluid shunt patency. *J Neurosurg* 1975; 42:728-730.
- Stein SC, Apfel S. A noninvasive approach to quantitative measurement of flow through CSF shunts. *J Neurosurg* 1981; 54:556-558.
- Hara M, Kadowaki C, Konishi Y, Ogashiwa M, Numoto M, Takeuchi K. A new method for measuring cerebrospinal fluid flow in shunts. *J Neurosurg* 1983; 58:557-561.
- Edelstein WA, Bottomley PA, Pfeifer LM. A signal-to-noise calibration procedure for NMR imaging systems. *Med Phys* 1984; 11:180-185.
- Hopkins AL, Yeung HN, Bratton CB. Multiple field strength in vivo T1 and T2 for cerebrospinal fluid protons. *Magn Reson Med* 1986; 3:303-311.
- Moran PR. A flow zeugmatographic interlace for NMR imaging in humans. *Magn Reson Imaging* 1982; 1:197-203.
- Bryant DJ, Payne JA, Firmin DN, Longmore DB. Measurement of flow with NMR imaging using a gradient pulse and phase difference technique. *J Comput Assist Tomogr* 1984; 8:588-593.
- Meier D, Maier S, Bosiger P. Quantitative flow measurements on phantoms and on blood vessels with MR. *Magn Reson Med* 1988; 8:25-34.
- Constantinesco A, Mallet JJ, Bonmartin A, Lallot C, Briguet A. Spatial or flow velocity phase encoding gradients in NMR imaging. *Magn Reson Imaging* 1984; 2:335-340.
- Nishimura DG, Macovski A, Pauly JM. Magnetic resonance angiography. *IEEE Trans Med Imaging* 1986; 5:140-151.
- Lenz GW, Haacke EM, Masaryk TJ, Laub G. In-plane vasculature imaging: pulse sequence design and strategy. *Radiology* 1988; 166:875-882.
- Mayo J, McVeigh ER, Hoffman N, Poon PY, Henkelman RM. Disappearing iliac vessels: a phase cancellation phenomenon. *Radiology* 1987; 164:555-557.
- Wedeen VJ, Rosen BR, Buxton R, Brady TJ. Projective MRI angiography and quantitative flow-volume densitometry. *Magn Reson Med* 1986; 3:226-241.
- Savader SJ, Savader BL, Murtagh FR, Clarke LP, Silbiger ML. MR evaluation of flow in a ventricular shunt phantom with in vivo correlation. *J Comput Assist Tomogr* 1988; 12:765-769.